

Tactile Synthesis and Perceptual Inverse Problems Seen from the View Point of Contact Mechanics

QI WANG and VINCENT HAYWARD

Haptics Laboratory, Center for Intelligent Machines, McGill University

A contact mechanics analysis was used to explain a tactile illusion engendered by straining the fingertip skin tangentially in a progressive wave pattern resulting in the perception of a moving undulating surface. We derived the strain tensor field induced by a sinusoidal surface sliding on a finger as well as the field created by a tactile transducer array deforming the fingerpad skin by lateral traction. We found that the first field could be well approximated by the second. Our results have several implications. First, tactile displays using lateral skin deformation can generate tactile sensations similar to those using normal skin deformation. Second, a synthesis approach can achieve this result if some constraints on the design of tactile stimulators are met. Third, the mechanoreceptors embedded in the skin must respond to the deviatoric part of the strain tensor field and not to its volumetric part. Finally, many tactile stimuli might represent for the brain an inverse problem to be solved, such specific examples of 'tactile metameres' are given.

Categories and Subject Descriptors: H.5.2 [**Information Interfaces and Presentation**]: User Interface-Haptic I/O; H.5.1 [**Information Interfaces and Presentation**]: Multimedia Information Systems, Artificial, augmented, and virtual realities; H.1.2 [**Models and Principles**]: User/Machine Systems Human information processing

General Terms: Human Factors, Theory

Additional Key Words and Phrases: Tactile synthesis, Computational tactile perception, Tactile transducers arrays, Contact mechanics, Tactile sensing, Lateral skin deformation, Haptics

1. INTRODUCTION

Artificially produced tactile sensations are needed for virtual reality [Hoffman et al. 1998], medical technologies [Dario et al. 2003], industrial applications [Kikuuwe et al. 2005], adaptive technologies for the blind and visually handicapped [Levesque et al. 2005], as well as in new portable human-machine interfaces [Pasquero et al. 2007]. Since touch plays a central role in human manipulation, lacking tactile sensations significantly impairs performance in those applications. In these examples, users could benefit from the replacement of natural sensations with artificially produced ones. The effectiveness of these systems depends on how efficiently tactile sensations can be created and on their realism. The design of tactile displays and the synthesis of signals to drive them are therefore central questions.

Supported by a Discovery Grant of the Natural Sciences and Engineering Research Council of Canada and a E. L. Adler Fellowship for Wang. The authors are with the Center for Intelligent Machines, McGill University, Montréal, Qc, H3A 2A7, Canada; email: hayward@cim.mcgill.ca. Permission to make digital/hard copy of all or part of this material without fee for personal or classroom use provided that the copies are not made or distributed for profit or commercial advantage, the ACM copyright/server notice, the title of the publication, and its date appear, and notice is given that copying is by permission of the ACM, Inc. To copy otherwise, to republish, to post on servers, or to redistribute to lists requires prior specific permission and/or a fee.

© 20YY ACM 0000-0000/20YY/0000-0001 \$5.00

Tactile displays should create sensations that replicate the sensations that arise naturally. Most current distributed tactile displays use actuators to mechanically deform the fingerpad skin in order to produce tactile sensations that are, with varying degrees, specific to each device [Bliss et al. 1970; Moy et al. 2000; Hayward and Cruz-Hernandez 2000; Wagner et al. 2004; Webster III et al. 2005; Kyung et al. 2005; Wang and Hayward 2006]. For a recent survey please see [Pasquero 2006].

Tactile synthesis, which is to the tactile sense what audio synthesis is to audition or computer graphics is to vision, is the process of computing spatio-temporal skin deformations and converting them into transducer signals that elicit specific sensations. Approaches are diverse. Moy et al. [2000] developed a tactile synthesis model for replicating the strain and stress field in the fingerpad caused by contacting an object using a display that operates with normal indentation. Lau et al. [2004] rendered tactile sensations by relaying the spatially distributed forces collected by tactile sensors through a tactile display which is composed of an array of mechanical pins driven vertically by RC servomotors. Allerkamp et al. [2007] proposed a vibration based tactile rendering strategy in order to display virtual fine surfaces.

Earlier, it was observed that certain surface skin strain patterns gave tactile sensations resembling scanning embossed surfaces, although the skin deformation had no normal component [Hayward and Cruz-Hernandez 2000; Levesque et al. 2005], or a very small amount of it [Nakatani et al. 2006]. Drawing from the results of Kikuuwe et al. [2005], we studied the case of an undulating surface sliding on a finger. We compared the strain that this surface generates at a fixed depth to the strain caused by a transducer comprising a set of discrete lateral traction surfaces programmed to cause a traveling wave of deformation at the surface. We then addressed the conjecture stated in Section 4.3 of Kikuuwe et al. [2005]: “[laterotactile displays] ... may be capable of generating a sensation equivalent to that generated by the normal displacement-type tactile display devices”. We found:

- that such ‘laterotactile’ displays could at a short distance inside a finger (≈ 1 mm) replicate the strain caused by a moving undulated surface,
- an approach to the synthesis of periodic tactile shapes and of isolated features,
- basic design constraints for laterotactile displays,
- the implication of the existence of an inverse problem that the brain appears to solve readily and other considerations regarding the role of contact mechanics.

1.1 Demonstrating The Illusion

When holding a plastic comb between the index finger and the thumb, see Figure 1, applying a gentle traveling stroke at mid-length of the comb’s teeth with a pen typically induces the tactile sensation of a moving embossed dot running under the index fingertip [Hayward and Cruz-Hernandez 2000].

Advantage was taken of this illusion in several projects. Recently, a 2D grid display was programmed to produce tactile graphics which consisted of two dimensional geometric forms represented by alignments of dots, space filling textures and vibrotactile regions in order to compose tactile symbols [Wang et al. 2006]. This demonstration was experienced by several hundreds of visitors at the ACM Conference on Human Factors in Computing Systems in April 2006.



Fig. 1. Manual demonstration of the “comb illusion” [Hayward and Cruz-Hernandez 2000]. An ordinary comb and a pencil is all what is needed. The pencil is used to deflect the teeth of the comb at mid-length in a stroking movement. A running embossing is typically felt despite the absence of normal skin deflection. Observers may easily notice that the illusion fails on the coarse side of the comb. Please see Section 2.6 for further comments on this.

The device used to create these sensations, the *STRESS*², is seen in Figure 2 [Wang and Hayward 2006].

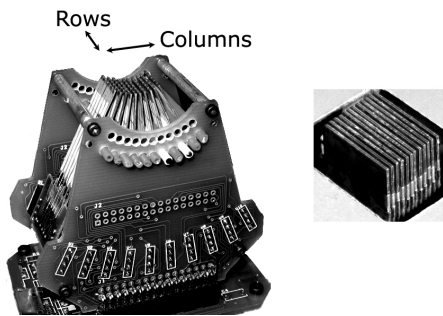


Fig. 2. View of the *STRESS*² (left). The display has ten by six independent “tractor” elements. Each of these independent tractors can be programmed to exert tangential traction on the skin. Deformation energy is provided by double-hinged bending piezoelectric benders [Wang and Hayward 2006]. Here, we consider a two-dimensional problem only, therefore, the stimulus is applied to all the elements of a column of tractors. A similar sensation results from using the 1-D virtual Braille display prototype VBD (right) [Levesque et al. 2005].

1.2 Empirical Tactile Synthesis Method Used

In the course of developing command signals for virtual braille display [Levesque et al. 2005], Levesque and Pasquero noticed that a traveling wave pattern caused observers to experience the sensation of an undulating surface. This effect was later leveraged for virtual tactile graphics [Wang et al. 2006].

Briefly, when the tactile transducer array moves across a displayed virtual sinusoidal surface, the deflection of each tractor is proportional to the height, see Figure 3. The resulting sensation is represented the lower part of the figure.

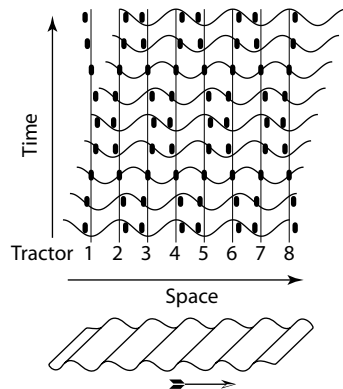


Fig. 3. When scanning a virtual surface, each tractor in a column—or each row of tractors—represented by thick dashes is programmed to move laterally as if it was sampling a traveling wave. This technique results in an oscillatory movement for each individual tractor with a fixed phase relationship with its neighbors. Bottom: Percept that the progressing wave pattern engenders. Note that there is no net movement of the display with respect to the skin.

Before us, several have attempted to study from first principles how tactile shape information can be extracted from strain sensors located beneath the skin surface. A common initial attack on the problem is to model the finger as a infinite linear elastic half space. Fearing and Hollerbach [1985] looked at the effect of indentation by a flat surface, a sharp edge and a corner and were able to make a number of important considerations regarding the basic requirements of the receptors [Fearing 1990]. Phillips and Johnson [1981b] developed a mechanical model of the skin to predict the responses of the mechanoreceptors embedded in the skin when deformed normally. With the exception of [Kikuuwe et al. 2005], these and more recent works, particularly [Ricker and Ellis 1993; Rossi et al. 1991], have considered only strain tensor fields caused by normal loads applied to the fingerpad.

Using the notation of [Kikuuwe et al. 2005], we now derive the strain tensor field caused by a sinusoidal surface sliding across the fingerpad as well as the field created by a tactile actuator array which deform the skin laterally. By comparing the two fields, we found that the first strain tensor field could be well approximated by the second field when tuning the parameters of the actuator array. This finding, therefore, provides a possible explanation for the illusion just mentioned. Using recent biomechanical data [Wang and Hayward 2007], we could find basic design parameters for a tractor array.

2. ANALYSIS USING CONTACT MECHANICS

The choice for studying the strain field rather than the stress field is justified by the fact that skin mechanoreceptors, in general, have been observed to be sensitive to a variety of strain patterns [Phillips and Johnson 1981a; LaMotte and Srinivasan 1987b; 1987a; Edin and Johansson 1995]. There is no reason to think that the skin mechanoreceptors are dominantly sensitive to stress because basic data suggest that the mechanical properties of these receptors do not differ greatly from that of the surrounding tissues [Wang et al. 1993; Laurent et al. 2002]. Only if the receptors in question were rigid relatively to the surrounding tissues that they could respond preferably to stress rather than to strain. In fact, that the mechanoreceptors be softer makes good engineering sense since it would establish a robust causal relationship between deformation and measurement, in much the same way that a strain gauge should be softer than the beam is it mounted on.

To make closed-form calculations possible we must assume that the fingerpad is a linear elastic homogeneous half-space. While it is well known that the skin is neither linear elastic nor homogenous, it is a reasonable assumption for the purpose of this paper. We assume that the compressibility of the fingerpad tissues where the receptors are embedded is small. It is actually the case that the embedding tissues are mostly made of incompressible water [Srinivasan et al. 1992]. We also must select the temporal and spatial periods of the mechanical signal to be well within the capabilities of the tactile system. Finally, we also need to assume that the tractors do not slip.

The assumption that laterotactile displays can deform the skin by lateral traction through friction is difficult to verify experimentally. Nevertheless, there are several lines of evidence to support it. Firstly, when a finger rests on a device like the STRESS² (Figure 2), approximately 40% of the skin area is still in contact.

When scanning objects, the skin deforms laterally [Levesque and Hayward 2003]. Amonton's law holds that the lateral force is invariant under large variations of the contact area, thus if natural traction created a deformation then it can be replicated by the display. Secondly, hundreds of observers had no difficulties experiencing the sensation depicted by Figure 3 if they pressed with the correct intensity (≈ 1 N).

This discussion brings about another observation. Laterotactile displays rely on the assumption of perfect traction. Conversely, indentation displays rely on the assumption of perfect slip to deform the skin in a predictable manner. The later assumption is less likely to hold in practice than the former. See Section 3.5.3 for further discussion on this point.

2.1 Nomenclature

\tilde{f}		Fourier transform of function f
$\delta(\cdot)$		Dirac's unit impulse function
$\epsilon^S(t, x, y), \tilde{\epsilon}^S(t, \xi, \eta)$		strain tensor at depth Z due to sliding surface
$\epsilon^T(t, x, y), \tilde{\epsilon}^T(t, \xi, \eta)$		strain tensor at depth Z due to a pair of line loads
η	m^{-1}	spatial frequency in the y direction
ξ	m^{-1}	spatial frequency in the x direction
ρ	m^{-1}	$\sqrt{\xi^2 + \eta^2}$
$\Phi(x)$	m^{-1}	shape of compressive component of $\epsilon^T(t, x, y)$
$\Psi(x)$	m^{-1}	shape of shear component of $\epsilon^T(t, x, y)$
ω	s^{-1}	temporal frequency
a, b		amplitude and width of a Gaussian function
A	m	half peak-to-peak amplitude of a sinusoidal surface
CNS		central nervous system
d	m	half inter-tractor distance
$D(\eta)$		$2\pi\delta(\eta)$
E	$\text{N}\cdot\text{m}^{-2}$	Young's modulus of the fingerpad
$\mathcal{F}(\cdot), \mathcal{F}(\cdot)^{-1}$		Fourier transform, inverse transform
$\tilde{\mathbf{G}}(\xi, \eta)$		spatial transfer function from surface displacement to strain at Z
$\tilde{\mathbf{g}}(\xi, \eta)$		$\tilde{\mathbf{G}}(\xi, \eta)[0 \ 0 \ 1]^\top$
$H(x, y), \tilde{H}(\xi, \eta)$	m	height of an undulating surface
i		$\sqrt{-1}$
k_1, k_2	m^{-1}	amplitude factors of approximated sinusoidal functions
$\tilde{\mathbf{K}}(\xi, \eta)$		spatial transfer function from line load to strain at Z
n		tractor index
p	m	spatial period of a sinusoidal surface
$\mathbf{q}(t, x, y), \tilde{\mathbf{q}}(t, \xi, \eta)$	$\text{N}\cdot\text{m}^{-1}$	tangential traction (lineic force)
$q(t), Q$	$\text{N}\cdot\text{m}^{-1}$	tangential traction amplitude, magnitude
$\mathbf{u}(t, x, y), \tilde{\mathbf{u}}(t, \xi, \eta)$	m	finger tip surface displacement
t	s	time
V	$\text{m}\cdot\text{s}^{-1}$	sliding velocity of sinusoidal surface along x
x	m	tangential spatial coordinate in the sliding direction
y	m	tangential spatial coordinate orthogonal to the sliding direction
z	m	depth spatial coordinate normal to the surface
Z	m	presumed depth of mechanoreceptors

2.2 Strain Tensor Field Generated by Slipping on a Sinusoidal Surface

A sinusoidal grating with period p and amplitude A , Figure 4, is represented by

$$H(x, y) = A \sin\left(2\pi \frac{x}{p}\right).$$

With ξ and η the spatial frequencies in x and y , its Fourier transform is

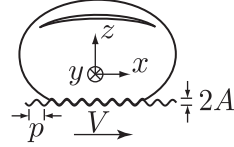


Fig. 4. A sinusoidal grating sliding across a fingerpad.

$$\tilde{H}(\xi, \eta) = i\pi A \left[\delta\left(\xi + \frac{2\pi}{p}\right) - \delta\left(\xi - \frac{2\pi}{p}\right) \right] (2\pi\delta(\eta)).$$

When the ridges move across the fingerpad at a constant speed V , the geometry of the fingerpad surface at the point (x, y) is presented by

$$\mathbf{u}(t, x, y) = h(x+Vt, y)[0 \ 0 \ 1]^\top = H(t, x, y)[0 \ 0 \ 1]^\top = A \sin\left(2\pi \frac{x+Vt}{p}\right) [0 \ 0 \ 1]^\top.$$

Posing $D(\eta) = 2\pi\delta(\eta)$ and using the Shift Theorem, we can derive its Fourier transform :

$$\begin{aligned} \tilde{\mathbf{u}}(t, \xi, \eta) &= e^{iVt\xi} \tilde{H}(\xi, \eta)[0 \ 0 \ 1]^\top \\ &= i\pi A e^{iVt\xi} \left[\delta\left(\xi + \frac{2\pi}{p}\right) - \delta\left(\xi - \frac{2\pi}{p}\right) \right] D(\eta)[0 \ 0 \ 1]^\top. \end{aligned}$$

The strain tensor field $\boldsymbol{\epsilon}^S(t, x, y)$ generated at a point (x, y, Z) , can be expressed in the spatial frequency domain [Kikuuwe et al. 2005]. Posing $\tilde{\mathbf{g}}(\xi, \eta) = \tilde{\mathbf{G}}(\xi, \eta)[0 \ 0 \ 1]^\top$:

$$\begin{aligned} \tilde{\boldsymbol{\epsilon}}^S(t, \xi, \eta) &= \mathcal{F}[\boldsymbol{\epsilon}^S(t, x, y)] \\ &= \tilde{\mathbf{G}}(\xi, \eta)\tilde{\mathbf{u}}(\xi, \eta) = \tilde{\mathbf{g}}(\xi, \eta)e^{iVt\xi}\tilde{H}(\xi, \eta) \\ &= \tilde{\mathbf{g}}(\xi, \eta) i\pi A e^{iVt\xi} \left[\delta\left(\xi + \frac{2\pi}{p}\right) - \delta\left(\xi - \frac{2\pi}{p}\right) \right] D(\eta), \end{aligned}$$

$$\begin{aligned} \text{where } \boldsymbol{\epsilon}^S(t, x, y) &= [\epsilon_{xx}^S \ \epsilon_{yy}^S \ \epsilon_{zz}^S \ \epsilon_{yz}^S \ \epsilon_{zx}^S \ \epsilon_{xy}^S]^\top, \\ \tilde{\mathbf{g}}(\xi, \eta) &= Ze^{-Z\rho} [\xi^2 \ \eta^2 \ -\rho^2 \ 2i\rho\eta \ 2i\rho\xi \ 2\xi\eta]^\top, \end{aligned}$$

$$\text{and } \rho = \sqrt{\xi^2 + \eta^2}.$$

$$\begin{aligned} \tilde{\boldsymbol{\epsilon}}^S(t, \xi, \eta) &= [\epsilon_{\xi\xi}^S \ \epsilon_{\eta\eta}^S \ \epsilon_{\zeta\zeta}^S \ \epsilon_{\eta\zeta}^S \ \epsilon_{\zeta\xi}^S \ \epsilon_{\xi\eta}^S]^\top \\ &= i\pi A e^{iVt\xi} \left[\delta\left(\xi + \frac{2\pi}{p}\right) - \delta\left(\xi - \frac{2\pi}{p}\right) \right] D(\eta) \\ &\quad Ze^{-Z\rho} [\xi^2 \ \eta^2 \ -\rho^2 \ 2i\rho\eta \ 2i\rho\xi \ 2\xi\eta]^\top. \end{aligned}$$

At constant depth Z , the first component of $\tilde{\epsilon}^S(t, \xi, \eta)$ then is:

$$\tilde{\epsilon}_{\xi\xi}^S = i\pi A e^{iVt\xi} \left[\delta\left(\xi + \frac{2\pi}{p}\right) - \delta\left(\xi - \frac{2\pi}{p}\right) \right] D(\eta) Z e^{-Z\rho} \xi^2.$$

Using the property of the Dirac function that $f(u)\delta(u - T) = f(T)\delta(u - T)$, the above expression can be rewritten

$$\tilde{\epsilon}_{\xi\xi}^S = \frac{2\pi^2 AZ i}{p^2} e^{-2\pi Z/p} 2\pi \left[e^{-i2\pi Vt/p} \delta\left(\xi + \frac{2\pi}{p}\right) - e^{i2\pi Vt/p} \delta\left(\xi - \frac{2\pi}{p}\right) \right] D(\eta).$$

Applying the inverse Fourier transform,

$$\epsilon_{xx}^S = \mathcal{F}^{-1}(\tilde{\epsilon}_{\xi\xi}^S) = \frac{4\pi^2 AZ}{p^2} e^{-2\pi Z/p} \sin\left(2\pi \frac{Vt + x}{p}\right).$$

Similarly, we could derive the other components of $\epsilon^S(t, x, y)$ as follows:

$$\begin{aligned} \tilde{\epsilon}_{\eta\eta}^S &= Z e^{-Z\rho} e^{iVt\xi} \left[\delta\left(\xi + \frac{2\pi}{p}\right) - \delta\left(\xi - \frac{2\pi}{p}\right) \right] D(\eta) \eta^2 = 0, \\ \epsilon_{yy}^S &= \mathcal{F}^{-1}[\tilde{\epsilon}_{\eta\eta}^S] = 0, \\ \tilde{\epsilon}_{\zeta\zeta}^S &= i\pi A Z e^{-Z\rho} e^{iVt\xi} \left[\delta\left(\xi + \frac{2\pi}{p}\right) - \delta\left(\xi - \frac{2\pi}{p}\right) \right] D(\eta) [-(\xi^2 + \eta^2)], \\ &= -\frac{i4\pi^3 AZ}{p^2} e^{-2\pi Z/p} \left[e^{-i2\pi Vt/p} \delta\left(\xi + \frac{2\pi}{p}\right) - e^{i2\pi Vt/p} \delta\left(\xi - \frac{2\pi}{p}\right) \right] D(\eta), \\ &= -\tilde{\epsilon}_{\xi\xi}^S, \\ \epsilon_{zz}^S &= \mathcal{F}^{-1}[\tilde{\epsilon}_{\zeta\zeta}^S] = -\epsilon_{xx}^S = -\frac{4\pi^2 AZ}{p^2} e^{-2\pi Z/p} \sin\left(2\pi \frac{Vt + x}{p}\right), \\ \tilde{\epsilon}_{\eta\zeta}^S &= i\pi A Z e^{-Z\rho} e^{i2\pi Vt\xi} \left[\delta\left(\xi + \frac{2\pi}{p}\right) - \delta\left(\xi - \frac{2\pi}{p}\right) \right] D(\eta) 2i\rho\eta = 0, \\ \epsilon_{yz}^S &= \mathcal{F}^{-1}[\tilde{\epsilon}_{\eta\zeta}^S] = 0 \\ \tilde{\epsilon}_{\zeta\xi}^S &= i\pi A Z e^{-Z\rho} e^{iVt\xi} \left[\delta\left(\xi + \frac{2\pi}{p}\right) - \delta\left(\xi - \frac{2\pi}{p}\right) \right] D(\eta) 2i\sqrt{\xi^2 + \eta^2} \xi, \\ &= \frac{8\pi^3 AZ}{p^2} e^{-2\pi Z/p} \left[e^{-i2\pi Vt/p} \delta\left(\xi + \frac{2\pi}{p}\right) + e^{i2\pi Vt/p} \delta\left(\xi - \frac{2\pi}{p}\right) \right] D(\eta), \\ \epsilon_{zx}^S &= \mathcal{F}^{-1}[\tilde{\epsilon}_{\zeta\xi}^S] = \frac{8\pi^2 AZ}{p^2} e^{-2\pi Z/p} \cos\left(\frac{2\pi(Vt + x)}{p}\right), \\ \tilde{\epsilon}_{\xi\eta}^S &= i\pi A Z e^{-Z\rho} e^{i2\pi Vt\xi} \left[\delta\left(\xi + \frac{2\pi}{p}\right) - \delta\left(\xi - \frac{2\pi}{p}\right) \right] D(\eta) \xi\eta = 0, \\ \epsilon_{xy}^S &= \mathcal{F}^{-1}[\tilde{\epsilon}_{\xi\eta}^S] = 0. \end{aligned}$$

In summary, the strain tensor field at depth Z generated by sliding on a sinusoidal surface is

$$\boldsymbol{\epsilon}^{\text{S}\top}(t, x, y) = \begin{bmatrix} \epsilon_{xx}^{\text{S}} \\ \epsilon_{yy}^{\text{S}} \\ \epsilon_{zz}^{\text{S}} \\ \epsilon_{yz}^{\text{S}} \\ \epsilon_{zx}^{\text{S}} \\ \epsilon_{xy}^{\text{S}} \end{bmatrix} = \frac{4\pi^2 AZ}{p^2} \begin{bmatrix} e^{-2\pi Z/p} \sin[2\pi(Vt + x)/p] \\ 0 \\ -e^{-2\pi Z/p} \sin[2\pi(Vt + x)/p] \\ 0 \\ 2e^{-2\pi Z/p} \cos[2\pi(Vt + x)/p] \\ 0 \end{bmatrix}. \quad (1)$$

Notice that the first and third entries are equal in magnitude and opposite in sign and the second, fourth and sixth entries are zero. Please see Section 3.5.2 for further comments on this observation. The reader will also notice that the strain tensor value is independent from the material properties.

2.3 Strain Tensor Field Generated by a Pair of Tractors

A pair of tractors deform the fingerpad skin laterally, as shown in Figure 5.

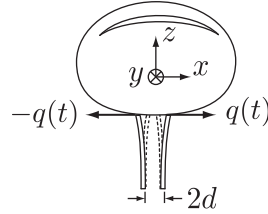


Fig. 5. A fingerpad laterally deformed by a pair of tractors.

The tangential tractions can be represented as line loads with mathematical description:

$$\mathbf{q}(t, x, y) = [-q(t)\delta(x + d) + q(t)\delta(x - d)][1 \ 0 \ 0]^\top$$

if d is half of the distance between the tractors. The Fourier transform of the tangential traction $\mathbf{q}(t, x, y)$ is:

$$\begin{aligned} \tilde{\mathbf{q}}(t, \xi, \eta) &= \mathcal{F}[\mathbf{q}(t, x, y)] \\ &= (-q(t)e^{id\xi} + q(t)e^{-id\xi}) D(\eta)[1 \ 0 \ 0]^\top. \end{aligned} \quad (2)$$

Kikuuwe et al. [2005] gave the spatial frequency domain representation of strain tensor induced at depth Z by a line load acting in lateral traction

$$\tilde{\boldsymbol{\epsilon}}^\top(t, \xi, \eta) = \tilde{\mathbf{K}}(\xi, \eta) \tilde{\mathbf{q}}(t, \xi, \eta), \quad (3)$$

where

$$\tilde{\mathbf{K}}(\xi, \eta) = \frac{3e^{-Z\rho}}{2E\rho^3} \begin{bmatrix} i\xi(\xi^2(1 - Z\rho) + 2\eta^2) & -i\xi^2\eta(1 + Z\rho) & Z\rho^2\xi^2 \\ -i\xi\eta^2(1 + Z\rho) & i\eta(2\xi^2 + \eta^2(1 - Z\rho)) & Z\rho^2\eta^2 \\ -i\rho^2\xi(1 - Z\rho) & -i\rho^2\eta(1 - Z\rho) & -Z\rho^4 \\ 2Z\rho^2\xi\eta & 2\rho^2(Z\eta^2 - \rho) & 2iZ\rho^3\eta \\ 2\rho^2(Z\xi^2 - \rho) & 2Z\rho^2\xi\eta & 2iZ\rho^3\xi \\ 2i\eta(\eta^2 - Z\rho\xi^2) & 2i\xi(\xi^2 - Z\rho\eta^2) & 2Z\rho^2\xi\eta \end{bmatrix}.$$

Combining (2) and (3), we obtain

$$\tilde{\epsilon}^{\text{T}\Gamma}(t, \xi, \eta) = \frac{3e^{-Z\rho}}{2E\rho^3} \begin{bmatrix} i\xi(\xi^2(1-Z\rho) + 2\eta^2) \\ -i\xi\eta^2(1+Z\rho) \\ -i\rho^2\xi(1-Z\rho) \\ 2Z\rho^2\xi\eta \\ 2\rho^2(Z\xi^2 - \rho) \\ 2i\eta(\eta^2 - Z\rho\xi^2) \end{bmatrix} (-q(t)e^{id\xi} + q(t)e^{-id\xi}) D(\eta).$$

Consequently,

$$\begin{aligned} \tilde{\epsilon}_{\xi\xi}^{\text{T}} &= \frac{3e^{-Z\rho}}{2E\rho^3} i\xi(\xi^2(1-Z\rho) + 2\eta^2) (-qe^{id\xi} + qe^{-id\xi}) D(\eta) \\ &= \frac{3e^{-Z|\xi|}}{2E\xi^2|\xi|} i\xi^3(1-Z|\xi|) (-qe^{id\xi} + qe^{-id\xi}) D(\eta). \end{aligned}$$

Its inverse Fourier transform can be found in closed form:

$$\begin{aligned} \epsilon_{xx}^{\text{T}} &= \frac{1}{4\pi^2} \int_{-\infty}^{\infty} \int_{-\infty}^{\infty} \tilde{\epsilon}_{\xi\xi}^{\text{T}} e^{i\xi x} e^{i\eta y} d\xi d\eta \\ &= \frac{1}{2\pi} \frac{3i}{2E} \left[\int_{-\infty}^0 \frac{e^{-Z|\xi|}}{|\xi|} \xi(1-Z|\xi|) (-q(t)e^{id\xi} + q(t)e^{-id\xi}) e^{i\xi x} d\xi \right. \\ &\quad \left. + \int_0^{\infty} \frac{e^{-Z|\xi|}}{|\xi|} \xi(1-Z|\xi|) (-q(t)e^{id\xi} + q(t)e^{-id\xi}) e^{i\xi x} d\xi \right] \\ &= \frac{1}{2\pi} \frac{3i}{2E} \left[\int_{-\infty}^0 \frac{e^{Z\xi}}{-\xi} \xi(1+Z\xi) (-q(t)e^{id\xi} + q(t)e^{-id\xi}) e^{i\xi x} d\xi \right. \\ &\quad \left. + \int_0^{\infty} \frac{e^{-Z\xi}}{\xi} \xi(1-Z\xi) (-q(t)e^{id\xi} + q(t)e^{-id\xi}) e^{i\xi x} d\xi \right] \\ &= \frac{3q(t)}{\pi E} \Phi(x), \end{aligned} \tag{4}$$

where

$$\begin{aligned} \Phi(x) &= \frac{1}{2} \left(\frac{x+d}{Z^2 + (x+d)^2} - \frac{x-d}{Z^2 + (x-d)^2} \right) \\ &\quad - Z^2 \left(\frac{x+d}{[Z^2 + (x+d)^2]^2} - \frac{x-d}{[Z^2 + (x-d)^2]^2} \right). \end{aligned}$$

Similarly

$$\begin{aligned}
 \tilde{\epsilon}_{\eta\eta}^T &= -\frac{3e^{-Z\rho}}{2E\rho^3}i\xi\eta^2(1+Z\rho)(-q(t)e^{id\xi}+q(t)e^{-id\xi})D(\eta)=0, \\
 \epsilon_{yy}^T &= \mathcal{F}^{-1}[\tilde{\epsilon}_{\eta\eta}^T]=0, \\
 \tilde{\epsilon}_{\zeta\zeta}^T &= -\frac{3e^{-Z|\xi|}}{2E|\xi|}i\xi(1-Z|\xi|)(-q(t)e^{id\xi}+q(t)e^{-id\xi})D(\eta) \\
 &= -\tilde{\epsilon}_{\xi\xi}^T, \\
 \epsilon_{zz}^T &= \mathcal{F}^{-1}[-\tilde{\epsilon}_{\xi\xi}^T] = -\epsilon_{xx}^T \\
 &= -\frac{3q(t)}{\pi E}\left[\frac{1}{2}\left(\frac{x+d}{Z^2+(x+d)^2}-\frac{x-d}{Z^2+(x-d)^2}\right)\right. \\
 &\quad \left.-Z^2\left(\frac{x+d}{[Z^2+(x+d)^2]^2}-\frac{x-d}{[Z^2+(x-d)^2]^2}\right)\right] \\
 &= -\frac{3q(t)}{\pi E}\Phi(x)
 \end{aligned}$$

and

$$\begin{aligned}
 \tilde{\epsilon}_{\eta\zeta}^T &= -\frac{3e^{-Z\rho}}{2E\rho^3}2Z\rho^2\xi\eta(-q(t)e^{id\xi}+q(t)e^{-id\xi})D(\eta)=0, \\
 \epsilon_{yz}^T &= \mathcal{F}^{-1}[\tilde{\epsilon}_{\eta\zeta}^T]=0, \\
 \tilde{\epsilon}_{\zeta\xi}^T &= \frac{3e^{-Z\rho}}{2E\rho^3}2\rho^2(Z\xi^2-\rho)(-q(t)e^{id\xi}+q(t)e^{-id\xi})D(\eta) \\
 &= \frac{3e^{-Z|\xi|}}{E|\xi|}(Z\xi^2-|\xi|)(-q(t)e^{id\xi}+q(t)e^{-id\xi})D(\eta).
 \end{aligned}$$

Applying methods similar to those used for equation (4), the inverse Fourier transform of $\tilde{\epsilon}_{\zeta\xi}$ could be derived:

$$\epsilon_{zx}^T = \frac{3q(t)}{\pi E}\Psi(x),$$

where

$$\begin{aligned}
 \Psi(x) &= Z\left(\frac{Z^2-(x-d)^2}{[Z^2+(x-d)^2]^2}-\frac{Z^2-(x+d)^2}{[Z^2+(x+d)^2]^2}\right) \\
 &\quad -\left(\frac{Z}{Z^2+(x-d)^2}-\frac{Z}{Z^2+(x+d)^2}\right).
 \end{aligned}$$

Since

$$\begin{aligned}
 \tilde{\epsilon}_{\xi\eta}^T &= -\frac{3e^{-Z\rho}}{2E\rho^3}2i\eta(\eta^2-Z\rho\xi^2)(-q(t)e^{id\xi}+q(t)e^{-id\xi})D(\eta)=0, \\
 \epsilon_{xy}^T &= \mathcal{F}^{-1}[\tilde{\epsilon}_{\xi\eta}^T]=0.
 \end{aligned}$$

In summary, the strain tensor field generated by a pair of tractors is

$$\epsilon^{\text{T}}(t, x, y) = \begin{bmatrix} \epsilon_{xx}^{\text{T}} \\ \epsilon_{yy}^{\text{T}} \\ \epsilon_{zz}^{\text{T}} \\ \epsilon_{yz}^{\text{T}} \\ \epsilon_{zx}^{\text{T}} \\ \epsilon_{xy}^{\text{T}} \end{bmatrix} = \frac{3q(t)}{\pi E} \begin{bmatrix} \Phi(x) \\ 0 \\ -\Phi(x) \\ 0 \\ \Psi(x) \\ 0 \end{bmatrix}. \quad (5)$$

2.4 Strain Tensor Field Generated by a Tractor Array

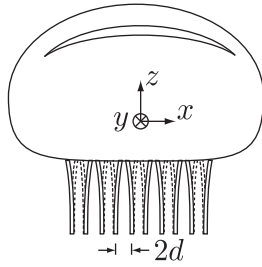


Fig. 6. A fingerpad laterally deformed by a tractor array.

Since the material is elastic and all governing equations are linear, the strain tensor field induced by a tractor array as in Figure 6 can be written

$$\epsilon^{\text{A}}(t, x, y) = \begin{bmatrix} \epsilon_{xx}^{\text{A}} \\ \epsilon_{yy}^{\text{A}} \\ \epsilon_{zz}^{\text{A}} \\ \epsilon_{yz}^{\text{A}} \\ \epsilon_{zx}^{\text{A}} \\ \epsilon_{xy}^{\text{A}} \end{bmatrix} = \frac{3q(t)}{\pi E} \begin{bmatrix} \sum_{n=-2}^2 \Phi(x - 4nd) \\ 0 \\ -\sum_{n=-2}^2 \Phi(x - 4nd) \\ 0 \\ \sum_{n=-2}^2 \Psi(x - 4nd) \\ 0 \end{bmatrix}. \quad (6)$$

2.5 Replication of two strain tensor fields

In a first step, we focused on the strain tensor field at a depth of $Z=1.25$ mm. This initial value was arrived at by considering that all mechanoreceptors are located roughly between depths 0.5 and 3 mm [Johnson 2001]. We found that $\sum_{n=-2}^2 \Phi(x - 4nd)$ approximates reasonably well a cosine function of the form $-k_1 \cos(2\pi x/(4d))$ and that $\sum_{n=-2}^2 \Psi(x - 4nd)$ is close to a sine function of the form $k_2 \sin(2\pi x/(4d))$. This observation can be appreciated in Figure 7. In our empirical tactile synthesis techniques, the tangential traction $q(t)$ is an ideal sinusoidal function $Q \sin(\omega t)$. This sine function can also be viewed as a sum:

$$q(t) = -Q \sin(\omega t) = -\frac{Q}{\sqrt{2}} \left[\cos\left(\omega t - \frac{\pi}{4}\right) + \sin\left(\omega t - \frac{\pi}{4}\right) \right].$$

A close comparison between ϵ_{xx}^{S} and ϵ_{xx}^{A} as well as comparison between ϵ_{xz}^{S} and ϵ_{xz}^{A} , which are listed below, might explain why observers feel a sinusoid surface when

their skin is laterally deformed in the manner described earlier.

$$\begin{aligned}\epsilon_{xx}^S &= \frac{4\pi^2 AZ}{p^2} e^{-2\pi Z/p} \sin\left(2\pi \frac{Vt+x}{p}\right) \\ &= \frac{4\pi^2 AZ}{p^2} e^{-2\pi Z/p} \left[\cos\left(2\pi \frac{x}{p}\right) \sin\left(2\pi \frac{Vt}{p}\right) + \sin\left(2\pi \frac{x}{p}\right) \cos\left(2\pi \frac{Vt}{p}\right) \right], \quad (7)\end{aligned}$$

$$\begin{aligned}\epsilon_{xz}^S &= \frac{8\pi^2 AZ}{p^2} e^{-2\pi Z/p} \cos\left(2\pi \frac{Vt+x}{p}\right) \\ &= \frac{8\pi^2 AZ}{p^2} e^{-2\pi Z/p} \left[-\sin\left(2\pi \frac{x}{p}\right) \sin\left(2\pi \frac{Vt}{p}\right) + \cos\left(2\pi \frac{x}{p}\right) \cos\left(2\pi \frac{Vt}{p}\right) \right], \quad (8)\end{aligned}$$

$$\begin{aligned}\epsilon_{xx}^A &\approx -k_1 \frac{3q(t)}{\pi E} \cos\left(2\pi \frac{x}{4d}\right) \\ &\approx \frac{3Qk_1}{\sqrt{2}\pi E} \left[\cos\left(2\pi \frac{x}{4d}\right) \sin\left(\omega t - \frac{\pi}{4}\right) + \cos\left(2\pi \frac{x}{4d}\right) \cos\left(\omega t - \frac{\pi}{4}\right) \right], \quad (9)\end{aligned}$$

$$\begin{aligned}\epsilon_{xz}^A &\approx k_2 \frac{3q(t)}{\pi E} \sin\left(2\pi \frac{x}{4d}\right) \\ &\approx -\frac{3Qk_2}{\sqrt{2}\pi E} \left[\sin\left(2\pi \frac{x}{4d}\right) \sin\left(\omega t - \frac{\pi}{4}\right) + \sin\left(2\pi \frac{x}{4d}\right) \cos\left(\omega t - \frac{\pi}{4}\right) \right]. \quad (10)\end{aligned}$$

If $k_2 = 2k_1$, when d and Z are well tuned, and when we let $d = p/4$, $\omega t = 2\pi Vt/p + \pi/4$ and $Q = (8\sqrt{2}\pi^3 AZE)/(3k_2 p^2) e^{-2\pi Z/p}$, then (9) and (10) can be rewritten as

$$\begin{aligned}\epsilon_{xx}^A &\approx \frac{4\pi^2 AZ}{p^2} e^{-2\pi Z/p} \left[\cos\left(2\pi \frac{x}{p}\right) \sin\left(2\pi \frac{Vt}{p}\right) + \cos\left(2\pi \frac{x}{p}\right) \cos\left(2\pi \frac{Vt}{p}\right) \right] \\ &\approx \frac{4\pi^2 AZ}{p^2} e^{-2\pi Z/p} \left[\cos\left(2\pi \frac{x}{p}\right) \sin\left(2\pi \frac{Vt}{p}\right) + \sin\left(2\pi \frac{x}{p} + \frac{\pi}{2}\right) \cos\left(2\pi \frac{Vt}{p}\right) \right], \quad (11)\end{aligned}$$

$$\begin{aligned}\epsilon_{xz}^A &\approx -\frac{8\pi^2 AZ}{p^2} e^{-2\pi Z/p} \left[\sin\left(2\pi \frac{x}{p}\right) \sin\left(2\pi \frac{Vt}{p}\right) + \sin\left(2\pi \frac{x}{p}\right) \cos\left(2\pi \frac{Vt}{p}\right) \right] \\ &\approx \frac{8\pi^2 AZ}{p^2} e^{-2\pi Z/p} \left[-\sin\left(2\pi \frac{x}{p}\right) \sin\left(2\pi \frac{Vt}{p}\right) + \cos\left(2\pi \frac{x}{p} + \frac{\pi}{2}\right) \cos\left(2\pi \frac{Vt}{p}\right) \right]. \quad (12)\end{aligned}$$

In equations (7) and (8), $\cos(2\pi x/p)$ and $\sin(2\pi x/p)$ represent the spatial components of a traveling wave, and $\sin(2\pi Vt/p)$ and $\cos(2\pi Vt/p)$ represent the temporal components. The first terms in the bracket of (7) and (11) are identical; so are the terms in the first bracket of (8) and (12). Nevertheless, by comparing the second terms in the bracket of ϵ_{xx}^S and ϵ_{xx}^A , we see that $\sin(2\pi x/p) \cos(2\pi Vt/p)$ has a phase difference of $\pi/2$ with $\sin(2\pi x/p + \pi/2) \cos(2\pi Vt/p)$. Similarly, the second term of the bracket of ϵ_{xz}^S and ϵ_{xz}^A , $\cos(2\pi x/p) \cos(2\pi Vt/p)$ and $\cos(2\pi x/p + \pi/2) \cos(2\pi Vt/p)$, have a phase difference of $\pi/2$ in the spatial domain.

The spatial period is $4d$. A $\pi/2$ phase difference translates into a distance of 0.6 mm for the current design of the STRESS² device. Previous works have shown that the minimum two-point discrimination distance in humans is ≈ 0.84 mm [Johnson and Phillips 1981; Lamb 1983]. This figure gives an estimate of how distant two events can be on the skin without being resolved. Under this threshold, the

mechanoreceptors stimulated by strain tensor ϵ^A provide the CNS with a similar information as when stimulated by tensor ϵ^S .

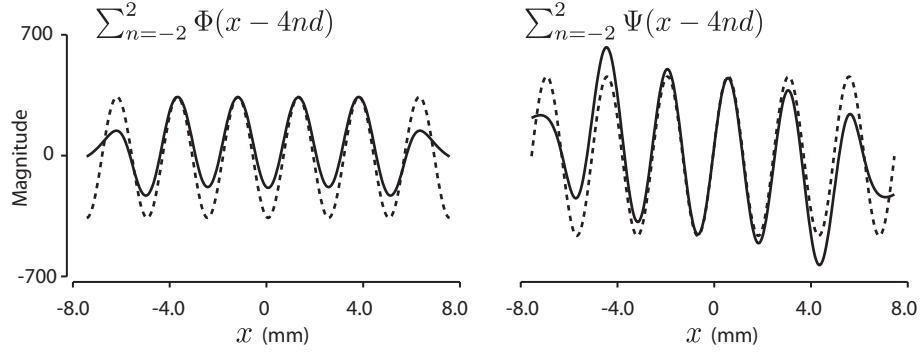


Fig. 7. Summed $\Phi(x)$ and $\Psi(x)$. Matched cos and sin functions in dashed lines.

2.6 Optimal d

We noticed that for some d and Z , the $\sum_{n=-2}^2 \Phi(x - 4nd)$ was an approximation of a cosine function, and $\sum_{n=-2}^2 \Psi(x - 4nd)$ was an approximation of a sine function. To let ϵ^A closely approximate ϵ^S , we now attempt find parameters that will minimize the discrepancy between $\sum_{n=-2}^2 3q(t)/(\pi E)\Psi(x - 4nd)$ and $-k_1 \cos(2\pi x/(4d))$ as well as between $\sum_{n=-2}^2 3q(t)/(\pi E)\Phi(x - 4nd)$ and $k_2 \sin(2\pi x/(4d))$. According to (1) and (6), the amplitude of $k_2 \sin(2\pi x/(4d))$ should be twice of that of $k_1 \cos(2\pi x/(4d))$, i.e. k_2 should be twice k_1 .

Focusing on the strain tensor field where $Z = 1.25$ mm and assuming that $p = 4d$, we should find the optimal tractor half spacing d_{opt} by minimizing:

$$d_{\text{opt}} = \operatorname{argmin}_d \left\{ \int_{-w/2}^{w/2} \left(\sum_{n=-2}^2 \Phi(x - 4nd) - \frac{k_2}{2} \cos\left(2\pi \frac{x}{4d}\right) \right)^2 dx + \int_{-w/2}^{w/2} \left(\sum_{n=-2}^2 \Psi(x - 4nd) - k_2 \sin\left(2\pi \frac{x}{4d}\right) \right)^2 dx \right\},$$

where for each d , k_2 is chosen to be:

$$k_2 = \frac{1}{2} \left\{ \max \left(\sum_{n=-2}^2 \Psi(x - 4nd); -4d \leq x \leq 4d \right) - \min \left(\sum_{n=-2}^2 \Phi(x - 4nd); -4d \leq x \leq 4d \right) \right\}.$$

Numerical optimization results show that when $Z = 1.25$ mm and for 10 mm of stimulated skin, d_{opt} is 0.938 mm. In order to effectively replicate the excitation ϵ^S with ϵ^A for mechanoreceptors located at depth 1.25 mm in the fingerpad skin,

the spatial period of the tactile transducer array should be $2d = 1.87$ mm. The approximations are illustrated in Figure 8.

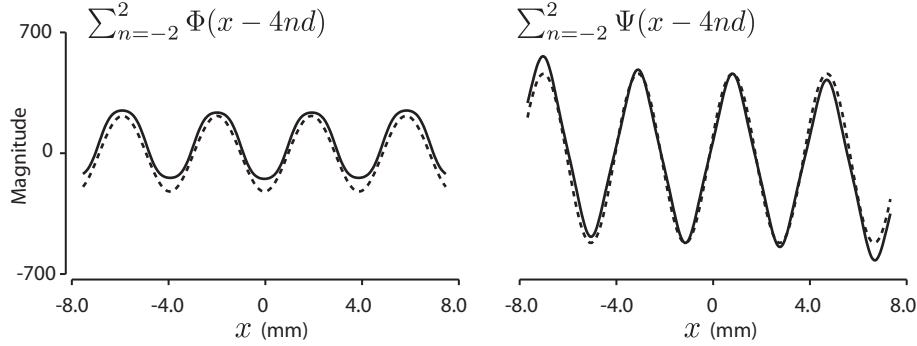


Fig. 8. Summed $\Phi(x)$ and $\Psi(x)$. Matched cos and sin functions in dashed lines.

The optimal display spatial period depends on Z . For instance, when $Z = 1$ mm, d_{opt} is 0.741 mm; when $Z = 0.75$ mm, d_{opt} is 0.634 mm. Our optimization results show that when Z is within 0.5 mm and 2 mm, d_{opt} is approximately proportional to Z , i.e. $d_{\text{opt}} \approx 0.75Z$ as seen in Figure 9.

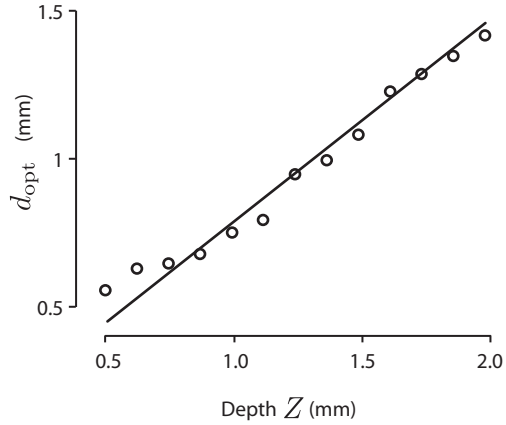


Fig. 9. The relationship between the depth Z and optimal d .

Referring back to the caption of Figure 1, it is possible to think that too coarse of a spatial period would cause a display to “miss” the target receptors by creating the optimal strain at the wrong depth.

3. DISCUSSION

3.1 Design constraints of the tactile displays based on lateral skin deformation

From Section 2.6, at a certain depth Z , the optimal d gives $\sum_{n=-2}^2 \Phi(x - 4nd) \approx -\frac{k_2}{2} \cos(2\pi x/(4d))$ and $\sum_{n=-2}^2 \Psi(x - 4nd) \approx k_2 \sin(2\pi x/(4d))$. However, k_2 is de-

terminated by Z and d . Moreover, within the depth range of interest, since the optimal $d = 0.75Z$, k_2 is thus, in turn, a function of Z .

According to (7), (11), (8), and (12), to reach the goal of using ϵ^A to approximate ϵ^S , the amplitude of ϵ_{xx}^A , ϵ_{yy}^A , and ϵ_{xz}^A should be identical to ϵ_{xx}^S , ϵ_{yy}^S , and ϵ_{xz}^S respectively, the amplitude Q of $q(t)$ should be

$$Q = \frac{8\sqrt{2}\pi^3 AZE}{3k_2 p^2} e^{-2\pi Z/p} = 1.60 \frac{AE}{k_2 Z}. \quad (13)$$

For an optimal d , that is, $d = d_{\text{opt}} \approx 0.75Z$, the $\sum_{n=-2}^2 \Psi(x - 4nd)$ exhibits a sinusoidal shape with period $4d$. Hence k_2 can be evaluated to be:

$$k_2 = \sum_{n=-2}^2 \Psi(x - 4nd) |_{x=d} = \frac{0.601}{Z}. \quad (14)$$

From (13), if $Z = 1.25$ mm and if E is taken to 1.54 MPa [Wang and Hayward 2007], in order to replicate the strain tensor field induced by a sinusoidal surface with an amplitude of 0.5 mm and a pitch of 4 mm, the amplitude of the tangential traction $q(t)$ should be $Q = 2$ N/mm. Seen another way, under the assumptions of linearity and homogeneity, the amplitude of the displayed sinusoid surface is

$$A = 0.625 \frac{k_2 Q Z}{E}.$$

To give scale, the maximum tangential traction of each millimetric-size actuator in a tactile array of the type STRESS² is 0.1 N/mm. The maximum amplitude of the displayed sinusoidal surface would be 0.024 mm.

Combining (13) and (14) gives

$$AE = 0.37 Q,$$

an expression that does not depend on Z and which expresses a *fundamental* tradeoff between the skin's material properties, the amplitude of the sensation and the lineic strength of the tractors.

From Section 2.5, we know that the strain tensor component ϵ_{xx}^A , ϵ_{yy}^A , and ϵ_{xz}^A exhibits a sinusoidal shape with period of $4d$ for a periodic sinusoidal traveling wave. Therefore, the period of the surfaces that the tactile transducer array can replicate is a multiple of $4d$ with a minimal period of $4d$. The spatial frequency $1/(4d)$ may be viewed as the spatial Nyquist frequency of the display system.

The temporal component of the strain tensor ϵ^A is $q(t)$ and of its counterpart ϵ^S have a temporal frequency Vt/p . The $q(t)$ was seen to yield the sum of two sinusoidal signals. The result is a $\pi/4$ phase lag between the real sinusoid surface and the virtual sinusoid surface. To confuse the CNS, d should be smaller than 0.84 mm. Consequently, the deepest mechanoreceptors that the tractor array can optimally stimulate is 1.12 mm. The targeted receptors believed to contribute to texture perception are less than 1 mm deep [Johnson 2001].

3.2 Synthesis of a Periodic Surface

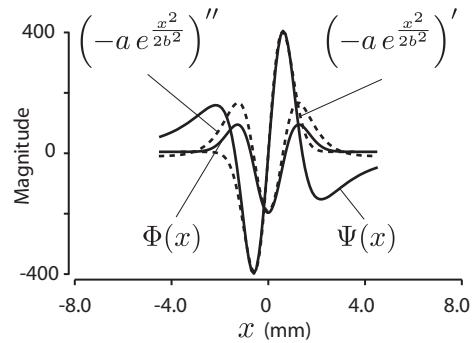
By the Fourier Theorem a laterotactile display can replicate any periodic surface. But of course, the reconstruction is subject to the usual limitations, namely, that

superposition applies and that aliasing can be controlled. Kikuuwe et al. [2005] analyzed in some depth the effects of aliasing in a laterotactile display. They concluded that in certain cases aliasing could reinforce the signal in a manner which would not be desirable in a general purpose display but they also noted that the footprint of the tractors created a low-pass effect which could attenuate high spatial frequencies. It is therefore likely that an optimal traction footprint could be found to create a desired amount of roll-off in view of optimizing reconstruction fidelity.

3.3 Synthesis of an Isolated Features

The internal strain caused by a pair of surface tractors has also very interesting characteristics. In Figure 10 the ‘compressive’ and ‘shear’ components of the strain tensor ϵ^T (equation (5), $\Phi(x)$ and $\Psi(x)$ respectively), are plotted for $Z = 1.25$ mm and $d = 0.6$ mm. A rough optimization done by matching the extrema of the first and second derivative of a Gaussian function indicates an intriguing resemblance of $\Phi(x)$ with the second derivative of a Gaussian and of $\Psi(x)$ with the first derivative. This strain pattern also resembles that caused by a variety of indentation conditions [Ricker and Ellis 1993]. This observation implies that the contact mechanics of a pair of tractors, like that of punch indentation, have band-pass filter characteristics, something also noted by Kikuuwe et al. [2005]. Having an array of programmable tractors effectively creates a bank of spatial filters with varying bandwidths. This fact merits further investigation because of the potential it affords for the synthesis of isolated tactile features such as dots or edges.

Fig. 10. The solid lines show plots of $\Phi(x)$ and $\Psi(x)$ for $Z = 1.25$ mm and $d = 0.6$ mm. In the dashed lines, plots of the first and second derivative of a Gaussian scaled to match the extrema.



3.4 Implications For the Design of Tactile Displays

To display an undulating surface of a given amplitude, the traction applied tangentially should be sufficient. Our current STRESS² tactile display could reliably generate strong virtual tactile texture although, theoretically, the maximum height of the virtual sinusoidal surface rendered by the STRESS² is 0.024 mm, see Equation (13). This discrepancy might be attributed to the following possibilities.

Humans are sensitive to very small amplitude textures; LaMotte and Whitehouse [1986] reported that subjects could reliably detect embossed dots 0.55 mm in diameter but only 0.003 mm in height. For mathematical convenience, we have ignored the fact that the skin is neither linear elastic, nor homogenous, nor isotropic. In

particular, the geometry of the epidermal ridges, dermal papillae, and epidermal pegs has for a long time attracted the attention of researchers as a possible tactile amplification mechanism [Cauna 1954; Phillips and Johnson 1981b; Maeno et al. 1998; Gerling and Thomas 2005].

By the same token, the actual biomechanical structure of the skin might require the optimal display spatial period to be somewhat different from that predicted by our linear analysis. It is our experience that if a display is too coarse or too tight it becomes inefficient. A true optimum remains to be found.

It is a very difficult problem to predict the impact of the structure and mechanics of the biological skin on the validity of the assumptions made to carry out the calculations. In the simplest case, the effect of this mechanics could be expressed as a sensitivity enhancement. It is more likely that they give rise to new behaviors that cannot be expressed with a linear model. Nevertheless the linear model explains the behavioral effects we have observed surprisingly well for the case of the simple shapes we have explored. The potential discovery of new effects justifies the investigation of more refined models.

3.5 Implication for the Human Tactile Sensing System

3.5.1 *Gaussian Filters.* The natural strain mechanics create transfer functions kernels from surface deformation to deformation in the regions where the receptors are located that resemble the first and second derivative of Gaussian functions. This holds whether surface deformation is by indentation or by differential traction. This fact is highly intriguing. A comparison with the visual system [Marr and Hildreth 1980], even if speculative, is almost inescapable. In particular, it could be hypothesized that the detection of sharp changes at the surface could be detected by zero crossings of the shear component inside the skin and that this basic mechanism could operate at different scales according to the depths at which the receptors are located. This simple mechanism would create a vast ensemble of filters optimally tuned for different scales both in time and in space [Marr and Hildreth 1980].

3.5.2 *Deformations picked up by the mechanoreceptors.* The strain tensor expressions (1) and (6) have the characteristic that the first and third entries are equal in magnitude and opposite in sign. This particularity expresses that volume is conserved as a result of the incompressibility property of tissues. A consequence is that the volumetric part of the deformation tensor contains no information which, in turn, implies that a *change in pressure* has no effect on tactile sensing (a common observation of deep divers or when dipping a finger in a glass of mercury). Therefore, the deviatoric part is left entirely to hold the quantities responsible for sensing. Saying that touch is the result of “pressure” is an incomplete statement. Touch is the result of the non-uniform distribution of pressure *and/or* of traction at the surface of the skin, the only quantities able to affect the deviatoric parts of the strain fields in the skin tissues. In fact, our displays operate without any pressure change whatsoever.

3.5.3 *Existence of an Inverse Problem for the CNS to Solve.* One of our purposes was to show that the seemingly simple and serendipitously found synthesis method:

perceptual surface height \rightarrow physical lateral deflection,

appears to work as the result of the combination of a rather complex phenomenon in contact mechanics and of basic limitations of the human tactile system. This map is not one-to-one but rather one-to-many since other methods of rendering can also be effective. We now know at least two methods: stimulating the skin with a frictionless undulated surface or stimulating the skin with a fully adhesive surface deforming laterally in a progressive wave pattern. There must exist, therefore, an infinity of possibilities between these two extremes, neither of which is quite ecological. This infinitum could be generated, for example, by continuous interpolation between the boundary conditions of these two *limiting cases*. Naturally occurring loading conditions must lie between these two extremes. In fact, experimental evidence indicates that natural stimuli, such as raised features, give rise to skin deformations that are a combination of normal and lateral deformation [Levesque and Hayward 2003]. The CNS, therefore, must be solving a version of:

strain field \rightarrow perceptual surface height,

where the same strain field can arise from contact with very different objects *and* also from many different contact conditions, yet arriving at a unique solution. This indicates the existence of *tactile metameres* so named here by analogy with visual metameres for color, size, or shape. Furthermore, the fundamentally ambiguous nature of tactile stimulation may help explain why virtual surfaces created by traction feel higher than predicted by the analysis of limiting cases.

It is therefore a challenge to characterize this problem further and the manner in which it can be solved. It is already known that different indentation patterns give rise to similar strain fields such as the “confounders” of Ricker and Ellis [1993]. Key insights into how this question might be approached can be found in the work of Ferrier and Brockett [2000] who described an algorithm that could solve a related problem using a membrane energy minimization principle and in the work of Rossi et al. [1991] who attempted to apply regularization theory to the indentation inversion problem.

4. CONCLUSION

In this paper, we intended to explain an illusion that has been used to various ends. The strain tensor field induced by a sliding sinusoidal surface and by a tractor array deforming the fingerpad skin laterally were derived. We found that the first strain tensor field could be well approximated by the second strain tensor field given some characteristics of a tactile display made of a tractor array are met. The intrinsic disparity of the two strain tensor fields might be masked by the spatial sensitivity limits of the human tactile system. The methods used in analysis could be used to develop other tactile rendering techniques.

Our analysis is, so far, quasi-static. Future research should be directed to the quantitative evaluation of the strain tensor fields considering the viscoelasticity and the actual structure of the skin using finite element or other methods. Design

optimization of tactile displays using lateral skin deformation principles could significantly improve performance. Furthermore, it will important to carry out more systematic psychophysical experiments to explore ways to minimize the effects of the intrinsic discrepancy between two strain tensor fields, or obtain new effects, for example, to increase contrast.

ACKNOWLEDGMENT

Vincent Levesque and the reviewers contributed many insightful comments which helped to improve this article considerably.

REFERENCES

- ALLERKAMP, D., BÖTTCHER, G., WOLTER, F.-E., QU, A. C. B., AND SUMMERS, I. R. 2007. A vibrotactile approach to tactile rendering. *The Visual Computer* 23, 2, 97–108.
- BLISS, J., KATCHER, M., ROGERS, C., AND SHEPARD, R. 1970. Optical-to-tactile image conversion for the blind. *IEEE Trans. on Man-Machine Systems* 11, 1, 58–65.
- CAUNA, N. 1954. Nature and functions of the papillary ridges of the digital skin. *The Anatomical Record* 119, 449–468.
- DARIO, P., HANNAFORD, B., AND MENCIASSI, A. 2003. Smart surgical tools and augmenting devices. *IEEE Trans. on Robotics and Automation* 19, 5, 782–792.
- EDIN, B. B. AND JOHANSSON, N. 1995. Skin strain patterns provide kinaesthetic information to the human central nervous system. *J. of Physiology* 487, 243–251.
- FEARING, R. S. 1990. Tactile sensing mechanisms. *International J. of Robotics Research* 9, 3, 3–23.
- FEARING, R. S. AND HOLLERBACH, J. M. 1985. Basic solid mechanics for tactile sensing. *International J. of Robotics Research* 4, 40–54.
- FERRIER, N. J. AND BROCKETT, R. W. 2000. Reconstructing the shape of a deformable membrane from image data. *International J. of Robotics Research* 19, 9, 795–816.
- GERLING, G. AND THOMAS, G. 2005. The effect of fingertip microstructures on tactile edge perception. In *First Joint Eurohaptics Conference and Symposium on Haptic Interfaces for Virtual Environment and Teleoperator Systems*. 63–72.
- HAYWARD, V. AND CRUZ-HERNANDEZ, M. 2000. Tactile display device using distributed lateral skin stretch. In *Proceedings of the Haptic Interfaces for Virtual Environment and Teleoperator Systems Symposium*. Vol. DSC-69-2. ASME, 1309–1314.
- HOFFMAN, H. G., HOLLANDER, A., SCHRODER, K., ROUSSEAU, S., AND FURNESS, T. 1998. Physically touching and tasting virtual objects enhances the realism of virtual experiences. *Virtual Reality* 3, 4, 226–234.
- JOHNSON, K. O. 2001. The roles and functions of cutaneous mechanoreceptors. *Current Opinion in Neurobiology* 11, 4, 455–461.
- JOHNSON, K. O. AND PHILLIPS, J. R. 1981. Tactile spatial resolution: I. two-point discrimination, gap detection, grating resolution, and letter recognition. *J. of Neurophysiology* 46, 1177–1192.
- KIKUUWE, R., SANO, A., MOCHIYAMA, H., TAKESUE, N., AND FUJIMOTO, H. 2005. Enhancing haptic detection of surface undulation. *ACM Trans. on Applied Perception* 2, 1, 46–67.
- KYUNG, K.-U., AHN, M., KWON, D.-S., AND SRINIVASAN, M. 2005. A compact broadband tactile display and its effectiveness in the display of tactile form. In *First Joint Eurohaptics Conference and Symposium on Haptic Interfaces for Virtual Environment and Teleoperator Systems, 2005*. 600–601.
- LAMB, G. D. 1983. Tactile discrimination of textured surfaces: psychophysical performance measurements in humans. *J. of Physiology* 338, 551–565.
- LAMOTTE, R. H. AND SRINIVASAN, M. A. 1987a. Tactile discrimination of shape: Responses of rapidly adapting mechanoreceptive afferents to a step stroked across the monkey fingerpad. *J. of Neuroscience* 7, 1672–1681.

- LAMOTTE, R. H. AND SRINIVASAN, M. A. 1987b. Tactile discrimination of shape: Responses of slowly adapting mechanoreceptive afferents to a step stroked across the monkey fingerpad. *J. of Neuroscience* 7, 1655–1671.
- LAMOTTE, R. H. AND WHITEHOUSE, J. 1986. Tactile detection of a dot on a smooth surface: peripheral neural events. *J. of Neurophysiology* 56, 1109–28.
- LAU, C. K. L., WAGNER, C. R., AND HOWE, R. D. 2004. Algorithms for tactile rendering in compliant environments. In *Proc. 12th International Symposium on Haptic Interfaces for Virtual Environment and Teleoperator Systems (HAPTICS'04)*. 32–39.
- LAURENT, V. M., HÉNON, S., PLANUS, E., FODIL, R., BALLAND, M., ISABEY, D., AND GALLET, F. 2002. Assessment of mechanical properties of adherent living cells by bead micromanipulation: Comparison of magnetic twisting cytometry vs optical tweezers. *J. of Biomechanical Engineering* 124, 4, 408–421.
- LEVESQUE, V. AND HAYWARD, V. 2003. Experimental evidence of lateral skin strain during tactile exploration. In *Proceedings of Eurohaptics 2003*. 261–275.
- LEVESQUE, V., PASQUERO, J., HAYWARD, V., AND LEGAULT, M. 2005. Display of virtual Braille dots by lateral skin deformation: Feasibility study. *ACM Trans. on Applied Perception* 2, 2, 132–149.
- MAENO, T., KOBAY-ASHI, K., AND YAMAZAKI, N. 1998. Relationship between the structure of human finger tissue and the location of tactile receptors. *JSME International J.* 41, 94–100.
- MARR, D. AND HILDRETH, E. 1980. Theory of edge detection. *Proceedings of the Royal Society of London, Series B, Biological Sciences* 1167, 187–217.
- MOY, G., SINGH, U., TAN, E., AND FEARING, R. 2000. Human psychophysics for teletaction system design. *Haptics-e* 1, 3.
- MOY, G., WAGNER, C., AND FEARING, R. S. 2000. A compliant tactile display for teletaction. In *Proceedings of the IEEE International Conference on Robotics and Automation*. 3409–3415.
- NAKATANI, M., HOWE, R. D., AND TACHI, S. 2006. The fishbone tactile illusion. In *Proceedings of Eurohaptics*. 69–73.
- PASQUERO, J. 2006. Survey on communication through touch. Tech. Rep. TR-CIM 06.04, Center for Intelligent Machines - McGill University.
- PASQUERO, J., LUK, J., LEVESQUE, V., WANG, Q., HAYWARD, V., AND MACLEAN, K. E. 2007. Haptically enabled handheld information display with distributed tactile transducer. *IEEE Trans. on Multimedia* 9, 4, 746–753.
- PHILLIPS, J. R. AND JOHNSON, K. O. 1981a. Tactile spatial resolution: II. neural representation of bars, edges, and gratings in monkey primary afferents. *J. of Neurophysiology* 46, 1192–1203.
- PHILLIPS, J. R. AND JOHNSON, K. O. 1981b. Tactile spatial resolution. III. a continuum mechanics model of skin predicting mechanoreceptor responses to bars, edges, and gratings. *J. of Neurophysiology* 46, 1204–1225.
- RICKER, S. L. AND ELLIS, R. E. 1993. 2-d finite-element models of tactile sensors. In *Proceedings of the IEEE International Conference on Robotics and Automation*. Vol. 1. 941–947.
- ROSSI, D. D., CAITI, A., BIANCHI, R., AND CANEPA, G. 1991. Fine-form tactile discrimination through inversion of data from a skin-like sensor. In *Proceedings of the IEEE International Conference on Robotics and Automation*. 398–403.
- SRINIVASAN, M. A., GULATI, R. J., AND DANDEKAR, K. 1992. In vivo compressibility of the human fingertip. In *Advances in Bioengineering, ASME Annual Winter Meeting*. Vol. 22. 573–576.
- WAGNER, C., LEDERMAN, S., AND HOWE, R. 2004. Design and performance of a tactile shape display using RC servomotors. *Haptics-e* 3, 4.
- WANG, N., BUTLER, J. P., AND INGBER, D. E. 1993. Mechanotransduction across the cell surface and through the cytoskeleton. *Science* 260, 1124–1127.
- WANG, Q. AND HAYWARD, V. 2006. Compact, portable, modular, high-performance, distributed tactile transducer device based on lateral skin deformation. In *Proceedings of the Symposium on Haptic Interfaces For Virtual Environment And Teleoperator Systems*. 67–72.
- WANG, Q. AND HAYWARD, V. 2007. In vivo biomechanics of the fingerpad skin under local tangential traction. *J. of Biomechanics* 40, 4, 851–860.

- WANG, Q., LEVESQUE, V., PASQUERO, J., AND HAYWARD, V. 2006. A haptic memory game using the STReSS² tactile display. In *Proceedings of the ACM 2006 Conference on Human Factors in Computing Systems, CHI 2006*. 271–274.
- WEBSTER III, R. J., MURPHY, T. E., VERNER, L. N., AND OKAMURA, A. M. 2005. A novel two-dimensional tactile slip display: design, kinematics and perceptual experiments. *ACM Trans. on Applied Perception* 2, 2, 150–165.